Taylor & Francis
Taylor & Francis Group

Canadian Journal of Remote Sensing
Journal canadien de télédétection

ISSN: 0703-8992 (Print) 1712-7971 (Online) Journal homepage: https://tandfonline.com/loi/ujrs20

# Characterization of Combined Effects of Urban Built-Up and Vegetated Areas on Long-Term Urban Heat Islands in Beijing

Chengming Ye, Rui Chen, Yao Li, Tianqiang Liu, Keli Diao & Jonathan Li

**To cite this article:** Chengming Ye, Rui Chen, Yao Li, Tianqiang Liu, Keli Diao & Jonathan Li (2019): Characterization of Combined Effects of Urban Built-Up and Vegetated Areas on Long-Term Urban Heat Islands in Beijing, Canadian Journal of Remote Sensing, DOI: 10.1080/07038992.2019.1644157

**To link to this article:** https://doi.org/10.1080/07038992.2019.1644157

CANADIAN JOURNAL OF REMOTE SENSING
https://doi.org/10.1080/07038992.2019.1644157



# Characterization of Combined Effects of Urban Built-Up and Vegetated Areas on Long-Term Urban Heat Islands in Beijing

Chengming Ye[a], Rui Chen[a], Yao Li[b], Tianqiang Liu[a], Keli Diao[a], and Jonathan Li[c,d]

[a]MoE Key Laboratory of Earth Exploration and Information Technology, Chengdu University of Technology, Chengdu, 610059, China; [b]Institute of Mountain Hazards and Environment, Chinese Academy of Sciences, Chengdu, 610059, China; [c]Department of Geography and Environmental Management and Department of Systems Design Engineering, University of Waterloo, Waterloo, ON N2L 3G1, Canada; [d]Fujian Key Laboratory of Sensing and Computing for Smart Cites, Xiamen University, Xiamen, 361005, China

**ABSTRACT**

With the development of urbanization and industrialization, megacities have experienced more severe surface urban heat island (SUHI) effects. Land surface temperatures (LSTs) are retrieved; spatial distribution of temperature is characterized, and the relationship among temperatures or SUHIs and land-use and land cover (LULC) in Beijing City are discussed. The changing LSTs in Beijing, from 1990 to 2017, were calculated by a radiative transfer equation and mono-window algorithm. To estimate the effect of SUHI, Landsat-8 Thermal Infrared Sensor (TRIS) and Landsat-5 Thematic Mapper (TM) data were selected. There is an increasing trend toward high LSTs for different LULC types. The connection with building and vegetation density is analyzed. Results indicate that for every 1% increase in the density of buildings, the increase in amplitude of temperature in 2017 was twice as large as it was in 1995 for the study area. In terms of normalized difference vegetation index (NDVI) values, the decrease in amplitude of LST was 10 times that of the year 1995, where there is only a slight increase in the NDVI values of the area.

**RÉSUMÉ**

Avec le développement de l'urbanisation et de l'industrialisation, les mégapoles subissent des effets d'îlot de chaleur assez sévères. L'article décrit la température de surface (LST) de Beijing et discute la relation entre la distribution de la température et la couverture du sol (LULC) sur la base d'étude de répartition spatiale de la température de surface. Les variations de température au niveau de la surface de la ville de Beijing de 1990 à 2017 ont été calculées au moyen d'une équation de transfert de rayonnement et d'un algorithme à fenêtre unique. Pour se faire, les données du capteur infrarouge thermique Landsat-8 (TRIS) et TM de Landsat-5 ont été traitées. La tendance générale est une augmentation des températures de surface. La relation entre la température de surface et la densité des constructions et de la végétation a aussi été analysée. Pour chaque augmentation de 1% de la densité des constructions, l'amplitude de l'augmentation de la température en 2017 double par rapport à celle de 1995. L'amplitude de la température de surface (LST) diminue par un facteur de 10 en 2017 bien que l'augmentation de l'indice NDVI est faible.

**ARTICLE HISTORY**
Received 8 October 2018
Accepted 12 July 2019

## Introduction

Over the past few decades, the rapid urbanization and industrialization of cities has produced an effect, defined as urban heat island (UHI) (Ogashawara and Bastos 2012; Ye et al. 2017), where, during the day, compared to the surrounding suburban or rural areas (Jones and Lister 2010), the central districts of cities are almost always warmer and tend to remain so throughout the night. According to Hu et al. (2008), the UHI phenomenon, with its long-lasting urban thermal climate, imperceptibly influences our ecological environment and human living and health conditions. For instance, UHI engenders a reduction in a fraction of vegetation (Kaufmann et al. 2003) and the transpiration of water from plants (Bounoua et al. 2015). Furthermore, UHIs have had a severe impact on local weather and climate, altering local precipitation patterns, influencing air temperature and humidity, and increasing the rate of formation of high-temperature areas (Liu and Zhang 2011).

In general, the effect consists of 2 types: surface UHI and atmospheric UHI. Whereas a surface UHI

CONTACT Rui Chen chenruilxf@foxmail.com

can be reflected by land surface temperature (LST), a surface UHI is worse than an atmospheric UHI (Estoque et al. 2017). LST is one of the key metrics in global climatology and other research fields (Bechtel 2015). In research, the estimation of LST derived by thermal infrared remote sensing is widely used as a kind of auxiliary data to model air temperature (Şahin 2012; Cristóbal et al. 2008), characterize drought conditions and developments (Abbas et al. 2014; Orhan et al. 2014), and analyze the surface urban heat island (SUHI) (Melaas et al. 2016; Zipper et al. 2016). Also, it seems that changes from LST result from conditions leading to the formation of UHIs. Therefore, to assess the impact on SUHI effects, it is meaningful to derive the LST of a UHI, monitor the LST changes, and discuss the reasons for those changes.

Over the long term, research has shown there is a warming trend in LSTs, and the areas of high-temperature zones in cities are expanding annually (Ranagalage et al. 2017; Chen et al. 2016; Zhou et al. 2017; Knutson et al. 1999). Compared with the conventional method for collecting LSTs in situ using data from meteorological stations, satellite-based temperature measurements are more advantageous for global climate change studies and dynamic long-term observations over vast areas (Urban et al. 2013; Alavipanah et al. 2015). In addition, the technique is important for macroscopically analyzing the spatial distribution characteristics of LSTs. Sometimes, because of the low spatial resolution in image data, thermal remote sensing cannot be derived accurately. Orbital satellite data might be limited by image acquisition time and factors, such as nighttime and cloudy weather (Tomlinson et al. 2011).

Many previous studies focused on researching the factors affecting SUHI and the relationships between those factors. Latitude, relative position of land and sea, elevation, and seasons influence the differences in LSTs and SUHIs. However, only a few studies paid attention to the effect of SUHI or the new, more accurate and reasonable, method for the retrieval of LST. Regarding influencing factors, some researchers primarily found that although the relationship between a SUHI and LST is positive (Huang and Ye 2015; Ranagalage et al. 2017; Rinner and Hussain 2011; Chen et al. 2016), there is a positive exponential correlation with expansions of impervious surfaces (Xu et al. 2013). In addition, a few investigators, exploring the SUHI effect based on an analysis of land use and land cover (LULC), pointed out that the intensity of a SUHI depends on the spatial feature of the land cover (Wang et al. 2017; Zhou et al. 2017).

Besides climate, vegetation phenology, rainfall, solar radiation, and the other natural factors mentioned above, the human factors of socioeconomic development, such as the increase in the number of buildings, roads, gardens, and other surface-built objects, also influence changes in LST (Bechtel 2015). The main change in land cover, increased surface building, absorbs more heat from solar radiation, resulting in higher LSTs and eventually expanding the intensity of SUHIs. Urban and socioeconomic developments, as major factors influencing LULC changes, illustrate the spatial patterns of impervious surface and green spaces (Van and Bao 2010; Estoque et al. 2017). Martin et al. (2014) proposed a new alternative method, a thermal reference, surface intra-urban heat islands (SIUHIs), to characterize the effect of surface urban heat islands. To analyze the spatial distribution of UHIs, they selected seven different SIUHI categories based on the above-average LST for each pixel in a satellite image. Theoretically, LSTs extend continuously from urban centers to rural areas. Compared with SUHI, the new method eliminates the difficulty in distinguishing between urban and rural boundaries.

In fact, the characteristics of LSTs depend mainly on the distribution of urban vegetation and buildings. Many academic studies have used the normalized difference vegetation index (NDVI) and normalized difference building index (NDBI) to indicate vegetation density and building density, respectively. Moreover, the statistical analysis of the spatiotemporal variability of NDVI, NDBI, LST, and the relationships among them is essential in UHI studies (Zareie et al. 2016; Kumar and Shekhar 2015). Using satellite remote sensing data, all the retrievals of NDVI, NDBI, and LST can be calculated quickly (Tomlinson et al. 2011).

However, a single analysis of the trend in urban space development, population density, or other economic factors cannot reveal the complex relationship between urbanization and LST (Cui et al. 2016). The evaluation of urbanization dynamics and SUHI is very time-consuming (Chen et al. 2017). Furthermore, such studies comprehensively investigate the change combined with the energy policy, emission reduction plans, etc. (Choi et al. 2014). Nevertheless, instead of a simple linear relationship, it is difficult to describe quantitatively the changes in LST and explain the intrinsic connection. Still worthy of research is the establishment of a reasonable evaluation system for the impact of SUHI. A scientific system must be able

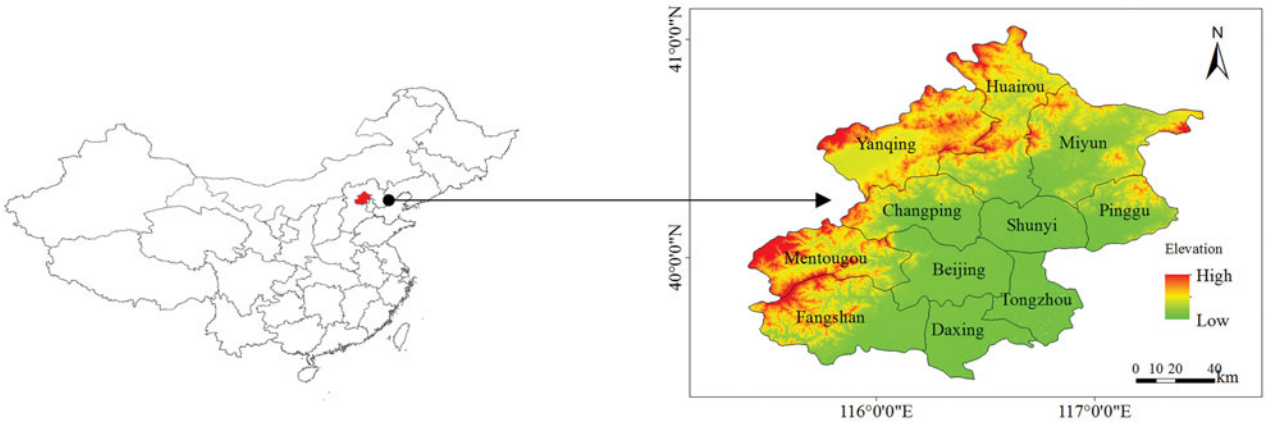


**Figure 1.** Location of the study area and elevation map of Beijing.

to quantify the effect of SUHI and the change in land-use types.

Based on the retrieval of LSTs, we propose dividing Beijing (our study area) into the following five levels according to relative temperature: very high, high, medium, low, and very low. Results show that each category will eventually have a certain ratio. The LSTs derived from remote sensing data for Beijing were determined 5 times (about once every 5 years) between 1990 and 2015 and, as an exception, in 2017. Likewise, using the remote sensing classification method, the study characterized the changes in LULC simultaneously with the LST. In this paper, for approximately the same level areas of temperature, we mainly discuss the LULC changes and the reasons for temperature change. On the contrary, significant research has been conducted regarding the protracted changes in LST that are influenced by the change in the land cover type for similar regions of interest. Finally, regarding changes in LULC, LST, and other changes, such as road conditions, water systems, and forest cover, our study focuses on the variety and relationships among these factors.

## Study area and data

### *Study area*

Beijing, the political and cultural center of China, whose center is located at 39°54′20″N and 116°25′29″E with a total area of 16,410.54 km$^2$, has developed into a modern international metropolis. With the climate belonging to the North Temperate Zone, Beijing has a typical semi-humid continental monsoon climate, with a hot and rainy summer, cold and dry winter, brief spring and autumn, and uneven distribution of precipitation.

The megacity is located at the northwestern edge of the North China Plain, backed by Mt. Yanshan, adjacent to Tianjin, and surrounded by Hebei Province. The north-western section of Beijing City, at a mean altitude of 43.5 m, where the altitude ranges from 20 m to 60 m in the plain area, but varies from 1,000 m to 2,000 m in other areas, is higher than the south-eastern section. The locations and elevations of different districts are shown in Figure 1, where the elevation data, reflected by digital elevation model (DEM) data, were acquired from ASTER GDEM, with a resolution of 30 m pixel.

In the past half century, as the capital of China, Beijing has undergone extensive urbanization to meet the needs of urban growth and sustainability (Wei and Ye 2014). In the past year, the city has been constructing a large number of buildings, roads, and piazzas, replacing the original land or soil with an urban built-up area of 1,401 km$^2$ (2016). The urbanization rate for Beijing, about 86.5% by the end of 2017, far exceeds that of other cities in China. As the city develops, it also incurs environmental problems, including the SUHI effect (Chen et al. 2017), water shortages, urban rainfall, and air pollution. Statistically, according to data from meteorological stations, from 1985 to 2010, the temperature in Beijing rose slowly with a downward trend in precipitation.

Rapid urbanization, which changes urban LULC and the spatial distribution of vegetation, exacerbates the increase in LST (Purwanto et al. 2016) and eventually changes the SUHI effect. LST is strongly influenced by urbanization characteristics (Song et al. 2017); consequently, the spatial characteristics of urbanization reflect the distribution of the SUHI effect. Therefore, to analyze the relationship between LST and the development of a city, it is essential to characterize the urbanization.

Table 1. Landsat-5 TM and Landsat-8 TRIS thermal images.

| Satellite data | Time (GMT) | Date | Resolution (m) |
|---|---|---|---|
| Landsat-5 TM | 02:13 | 18 September 1990 | 120 × 120 |
| Landsat-5 TM | 01:55 | 16 September 1995 | |
| Landsat-5 TM | 02:40 | 6 May 2005 | |
| Landsat-8 TRIS | 02:53 | 4 September 2014 | 100 × 100 |
| Landsat-8 TRIS | 02:53 | 28 September 2017 | |

### Satellite data

Our study used the thermal image satellite data provided by the USGS EROS Center and selected from Landsat-5 TM between 1990 and 2005 and Landsat-8 TRIS between 2014 and 2017 (see Table 1).

To avoid seasonal disturbances, the raster images for only the warmer seasons were acquired from the USGS website about once every 5 years. Only a small amount of image data is available under the experimental requirements that cloudless is essential in long-term sequence images for the same season. The longer the time of the image data spans, the more difficult it is to find available images for this research. While images with intervals of 5 years were collected as much as possible in the study, there were still some absences of images in 2000 and 2010, and only 1 image from Landsat 5 was obtained in May 2005, whereas the others were acquired in September.

Each image from Landsat-5 TM includes 7 bands, in which the sixth (thermal) band reflects the ground temperature with 120-m pixel resolution; resolution for the other bands is 30-m pixels. Standard Landsat-8 image data have bands from 2 sensors: OLI and TRIS. In the study, the selected band images with a resolution of 100-m pixel from TRIS are generally used for the retrieval of LST.

## Method

### Data preprocessing

Whereas the level 1 image data of Landsat has been geometrically corrected when acquired from the USGS, with a resolution of 30 m pixel for each band, before retrieving LSTs using satellite image data, it is essential to preprocess the data, including geometric correction, radiation calibration, and atmospheric correction. The original DN brightness values of all images were converted to atmospheric outer surface reflectance or brightness values reflecting absolute radiance.

Finally, to estimate LSTs, our study required the image data be converted into actual surface reflectance from radiance or surface reflectance by atmospheric correction.

### LST estimation

The most commonly used algorithms to retrieve LSTs from satellite data are of three types: radiative transfer equation (RTE), single-channel algorithm, and split-window algorithm. Taking into consideration the comparison of the above three algorithms conducted by Yu et al. (2014) and using Landsat-8 TRIS data, we selected the RTE algorithm to derive the LSTs because RTE has the highest accuracy compared with other methods. However, accurate LSTs, derived from Landsat-5 TM data, were achieved by the mono-window algorithm proposed by Qin et al. (2001, 2004).

It is worth noting that the radiative transfer equation algorithm was selected for Landsat 8, while the mono-window algorithm was selected for Landsat 5 to estimate LST, with the result that the inconsistent estimation with reality appeared possible. Meanwhile, to make the estimations using the 2 algorithms comparable, the relative LST was proposed to evaluate SUHI intensity and reduce the differences between results from 2 algorithms (see next section).

### Radiative transfer equation

First, the influence of the atmosphere on the surface thermal radiation must be estimated. Then, to obtain the surface thermal radiation intensity, the estimated atmospheric influence is subtracted from the total amount of thermal radiation observed by the satellite sensor. Finally, the thermal radiation intensity is converted to the corresponding LST.

The thermal infrared radiation brightness value, $L_\lambda$, observed by the satellite sensor, consists of 3 parts: (1) the upward radiance, $L^\uparrow$, from the atmosphere, (2) the real radiance from the ground to the satellite sensor after absorption by the atmosphere, and (3) the radiation reflected by the ground from the atmospheric downward radiation, $L^\downarrow$. The thermal infrared radiation brightness, $L_\lambda$, is expressed as follows:

$$L_\lambda = \left[\varepsilon B(T_s) + (1-\varepsilon)L^\downarrow\right]\tau + L^\uparrow \quad [1]$$

where ε is the surface emissivity derived by the NDVI threshold method proposed by Sobrino, and τ is the atmospheric transmission for the thermal infrared band acquired from the NASA website as the same as the other parameters, such as $L^\uparrow$ and $L^\downarrow$. $B(T_s)$ is the reference radiation brightness of the blackbody with a temperature of $T$. $T_s$ represents the real surface temperature, where $B(T_s)$ is calculated by the following:

$$B(T_s) = \left[L_\lambda - L^\uparrow - \tau(1-\varepsilon)L^\downarrow\right]/\tau\varepsilon \quad [2]$$

The next step is to calculate, using the Planck radiation formula, $T_s$ as the LST value expressed in the

following equation:

$$T_s = \frac{K_2}{\ln\left(\frac{K_1}{B(T_s)} + 1\right)} \quad [3]$$

where $K_1$ and $K_2$ are calibration constants.

### Mono-window algorithm

Based on the characteristics of surface thermal radiation conduction for the TM6 band, Qin et al. (2001) proposed a simple and feasible mono-window algorithm for the inversion of LST only from TM6 data. The mono-window algorithm requires the following 3 basic parameters: surface emissivity, atmospheric transmission, and average atmospheric temperature.

Before calculating LST, the DN value of the images recorded by the satellite sensor are converted to the surface radiation value as follows:

$$L_{(\lambda)} = L_{\min(\lambda)} + \left(L_{\max(\lambda)} - L_{\min(\lambda)}\right) Q_{dn}/Q_{\max} \quad [4]$$

where $L_{\max(\lambda)}$ and $L_{\min(\lambda)}$ are the radiation extremums that represent the maximum radiation intensity and the minimum radiation intensity, respectively, received by the sensor. $L_{(\lambda)}$ is the real intensity of radiation. $Q_{\max}$ is the maximum value of the pixel gray value. $Q_{dn}$ is the sampled pixel gray value of the image data. For Landsat-5 TM, the DN value is recorded by an 8-bit binary number, which means that $Q_{\max} = 255$.

In the next step, the pixel brightness temperature is calculated by the Planck function:

$$T_6 = \frac{K_2}{\ln\left(\frac{K_1}{L_{(\lambda)}} + 1\right)} \quad [5]$$

where $K_1$ and $K_2$ are the calibration constants, and $T_6$ is the brightness temperature of the image data.

The brightness temperature retrieved from the images is not the true surface temperature. Affecting the brightness temperature are the atmospheric and surface effects of thermal radiation, from which atmospheric radiation and absorption must be eliminated to calculate the true surface temperature.

Finally, $T_s$ is calculated by the mono-window algorithm consisting mainly of the following:

$$T_s = \{67.3554(C + D - 1) + [0.4414(C + D) + 0.4586]T_6 - DT_a\}/C \quad [6]$$

where $C = \varepsilon\tau$ and $D = (1 - \varepsilon)[1 + (1 - \varepsilon)\tau]$. $\varepsilon$ is the surface emissivity, which is calculated by the same method. $T_a$ is the average atmospheric, and $\tau$ is the atmospheric transmission. Both $T_a$ and $\tau$ are estimated based on atmospheric water content (or humidity) and the average temperature near the ground (Qin et al. 2003).

### Classification of LST intensity levels

Referring to similar denotations used by Kaufmann et al. (2003), to better analyze the change in the SUHI intensities in Beijing, we classified the estimated LSTs into 5 levels according to the deviation showing the different SUHI intensities. In our study, it was difficult to select remote sensing images less affected by the seasons. To ensure that the LSTs acquired from different years are comparable, we proposed graded surface temperatures, which eliminate the effects of some environmental factors, such as weather and seasons.

The 5 levels, in which the temperature of the area in each level changes within a certain range, are very high, high, medium, low, and very low. Each level occupies 20% of the total temperature domain, with the first level having the highest 20% of the temperatures and the other levels following suit. The relative LST intensity levels were selected to solve the problem for the effects on the difference between the estimations from 2 algorithms and the different atmospheric conditions in May and September.

After the estimation of LST, as for the same image, the frequency histogram of the LST was calculated to determine the change interval every time the LST values belonging to the highest outlier or the lowest outlier were removed. The change interval of LST for each image was divided uniformly into 5 inter-cells, and in the 5 cells of the LST interval, the first cell with the maximum LST is defined as very high temperature, and the others are high, medium, low and very low temperature in order.

### Classification of LULC types

According to the characteristics of LULC in Beijing, and using the original Landsat data with the resolution of 30 m, we classified LULC, with the traditional maximum likelihood classification method, into the following 5 types: vegetation, building sites, workshop buildings, water areas, and bare land. Based on the sample and reference data, the best classification result was selected. There is some difference between building sites and workshop buildings; the former refers to concrete buildings, such as roads, high-rise buildings and other pavements, whereas the latter refers to factory buildings, such as houses with steel tiles, of which the roof materials are generally

steel structures. Different LULCs respond to temperature differently. Apparently, vegetation and water areas often have relatively lower surface temperatures than the other types.

Here, a term was defined as ratio of the ecological configuration which refers to the proportion of the area with a certain type of LULC to the total area. More reasonable proportions of vegetation and buildings cannot only alleviate city's SUHI effect, but also promote the green development of urbanization.

In addition, in this study, to find the best ratio for the ecological configuration for medium-temperature areas, over time we monitored changes in land cover in areas with the same temperature levels. The change characteristics of LULC types in the same temperature level reflect the driving factors of the SUHI phenomenon. Different SUHI intensities have corresponding driving factors and have been affected by the different LULC types. Namely, when the LULC types of some area have changed, the change trend of SUHI could be forecast based on the driving factors and reasons known.

Urban areas with much vegetation often have low temperatures and weak SUHI intensities, thereby restricting the development of the city, whereas urban areas usually have strong SUHIs. LSTs in areas with the same land type change slowly, indicating that the ratio of different temperature levels changes as the vegetation and urbanization densities change. Increased building density and reduced vegetation coverage result in higher surface temperatures, causing more serious SUHIs.

### Division of building and vegetation density

Building density is denoted as the ratio of buildings per unit area. Areas of high building intensity may have higher LSTs, causing intense SUHIs, whereas the vegetation, represented by the average NDVI, usually has a negative effect on LST. NDVI, indicating the density of vegetation coverage, is expressed as follows:

$$NDVI = \frac{NIR - R}{NIR + R} \quad [7]$$

where $NIR$ and $R$ are the spectral reflectance of the near infrared (NIR) band and the red (R) band, respectively. When a region's $NDVI > 0.05$, it is considered that the vegetation areas and areas of high vegetation densities have higher NDVI values than building or water areas.

## Results and discussion

### Classification of LST and change trends of SUHI intensity

Figure 2 shows the spatial distribution of LSTs in Beijing from 1990 to 2017. The SUHI intensity in 2005 was more severe than that of 2014 and 2017 because there were more areas with bare land in 2005, resulting in high LSTs, where the spatial distribution characteristics of bare land are similar to those of the regions with high SUHI. Just as with building area, bare land also has a positive impact on high SUHI.

The spatial distribution of the areas with high elevations is similar to that of the areas with low LSTs. As seen in Figures 1 and 2, there is an obvious trend that some of the LSTs are negatively related to their elevation, reflecting that areas with very low LSTs mainly occur in mountains with high elevations.

Notably, a central urban area has a higher LST. As the areas with high LSTs expand, there is a greater temperature gap between urban and rural districts, where a threshold of building density was selected to divide the city into central urban areas and rural districts according to the sample statistics. Over the past 27 years, the percentage of areas with high LSTs increased from 7.95% to 17.35%. Especially, the building areas of Beijing experienced a greater increase in growth of 20.27%.

The image acquired in 2005 from Landsat-5 was selected to estimate LST for comparing the differences between the results from 2 algorithms. For Beijing city, the LST differences ranged from 0 to 3 °C, and the average difference value reached 1.16 °C (Figure 3). The spatial distribution characteristics of LST differences are closely related to the LULC types. The LST difference in the building area is mainly above 3 °C, while that in vegetation is maintained at 1 °C–2 °C. The LST estimations of the 2 algorithms are not much different, and the differences under different LULCs are consistent, which indicates that the relative LST may solve this problem that the different algorithms cause LST estimation differences.

### LST differences between LULCs

To illustrate the effect of different types of LULC on SUHI, we analyzed the spatial temperature distribution of buildings and vegetation for 1995, 2005, and 2017 (see Figure 4). An analysis over a 3-year period indicated rapid urbanization and overall rising urban temperatures.

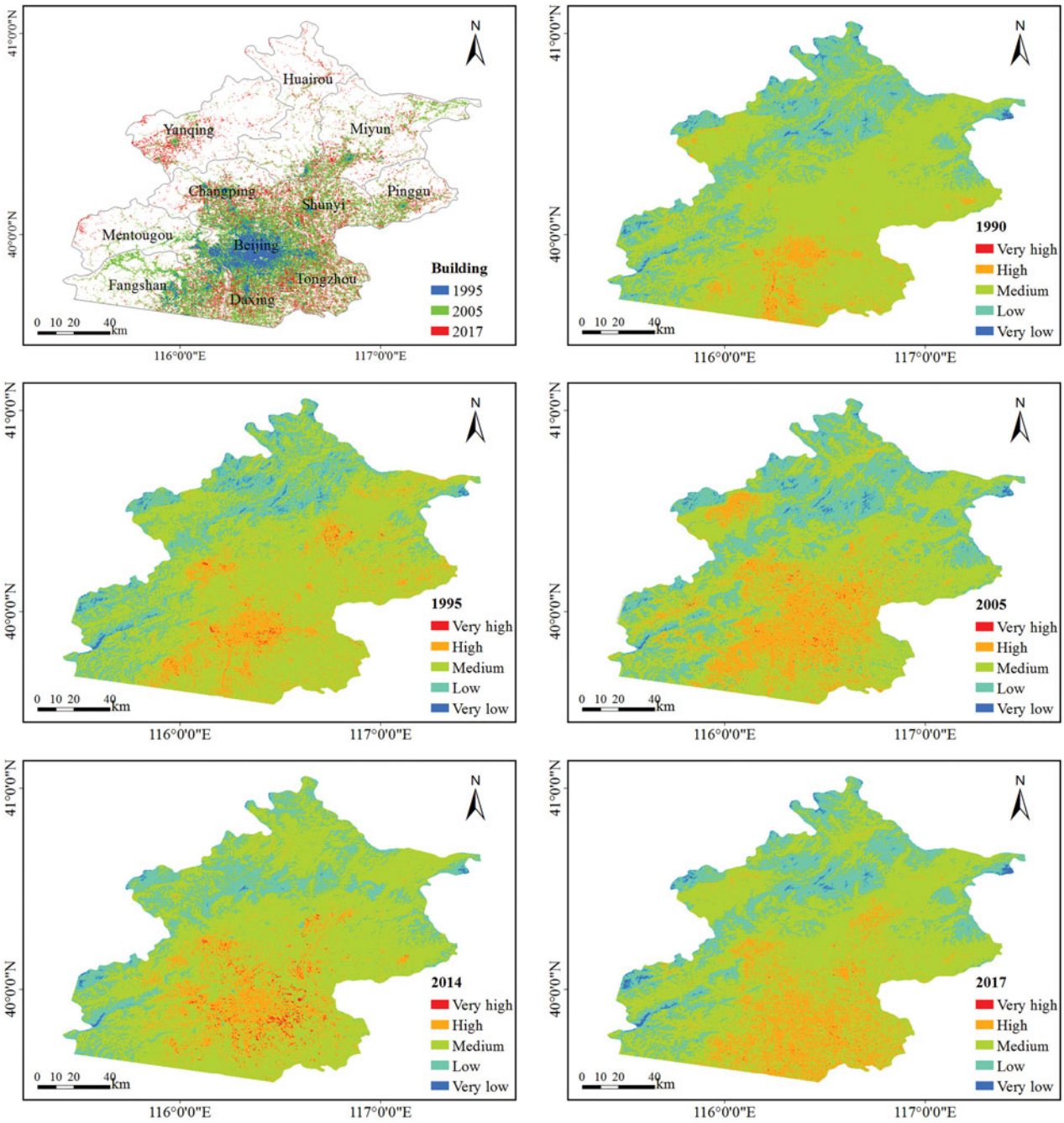


**Figure 2.** Change of building and the spatial distribution of LST in Beijing from 1990 to 2017.

Figure 4 reveals that the areas with high LSTs, distributed in the urban areas of Beijing city, have expanded, primarily to the southeastern plain area with low altitude. The area of buildings in Beijing has expanded rapidly with the increase in the high temperature ratio, while the area of vegetation has changed little and in 2017 had a lower temperature ratio than it did in 1995. Obviously, the spatial distribution characteristics of SUHI are similar for 1995, 2005, and 2017. From 1995 to 2017, building areas increased with rapid urbanization, where the area of high SUHI increased, but the proportion was reduced. However, vegetation areas did not change significantly in these 3 years, with a decrease in the trend of the area with low SUHI.

According to our statistics for the temperature distribution of different LULCs, there was an increasing trend in the high temperature ratio of buildings. Figure 5 shows the changes in the ratios of high, medium, and low temperatures among 4 land use types. The expansion of buildings and bare land is the main reason for high LSTs and UHIs. Therefore,

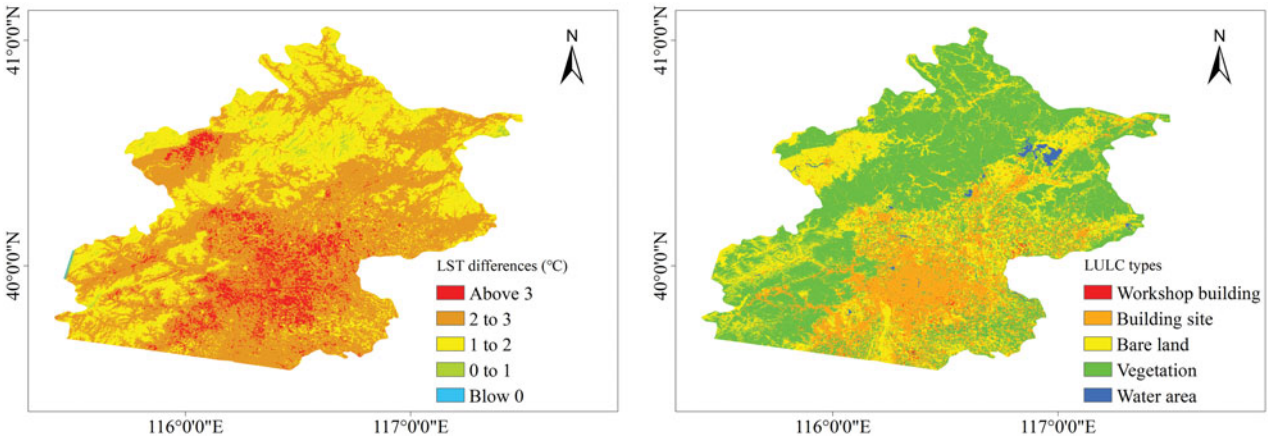


**Figure 3.** The LST differences between 2 algorithms (the LST estimation from the radiative transfer equation minus that from the mono-window algorithm) and the LULC types for 2005.

buildings and bare land always maintain a high or medium temperature, but only a small proportion of low temperatures.

On the contrary, vegetation and water areas have a low high-temperature ratio. In 1990, Beijing was 4.51% buildings, of which 61.41% were of high temperature with strong SUHI intensity. However, in 2017, only 22.40% of the buildings had 52.43% of the high-temperature areas. For vegetation, mainly distributed over the north-west of Beijing, the ratio of low-temperature areas increased from 30.27% to 64.40%. Notably, a mere 1.33% of water areas are areas of high temperature; the remainder are of medium and low temperatures.

### *LULC differences between LST intensity levels*

To explore the potential relationship between LULC types and LST, an analysis based on the distribution of land use types in areas with identical LST levels was also conducted. Figure 6 shows the distribution in 1995 and 2017 of LULC types in areas with high, medium, and low temperature. Between 1995 and 2017 in Beijing city, there was not much difference in the distribution characteristics of the high-temperature areas. In the same year of 1995 or 2017, high SUHI was driven by building area, whereas vegetation and water area have been leading low SUHI, reflecting the driving factors of the SUHI phenomenon with different levels. In the area with the same SUHI level, the area with high, medium, and low LST have changed slightly from 1995 to 2017.

However, with the development and expansion of the city from 1995 to 2017, building sites became the primary type of land use for the area, with their ratio increasing from 27.41% to 67.91%, replacing much of the vegetation, whose ratio dropped by 14.93%. The area of medium temperature, where vegetation occupied 75.38% of the proportion of 2017, increased significantly. Similarly, between 1995 and 2017, there was little change in the low-temperature areas, indicating that vegetation plays a prominent role in those areas. Sometimes, urban vegetation has a positive inhibitory effect on the UHI.

The type of land use that contributes most to a LST level is readily seen from the changes in the ratios of buildings, bare land, vegetation, and water areas at different LST levels shown in Figure 7. In the very high or high temperature areas, from 1990 to 2017, there was a large proportion of buildings and bare land and a slowly increasing trend in the ratio of buildings. Conversely, no matter what the year, vegetation is the main type of land use in the medium, low, and very low temperature areas.

### *Relationship between LST and building and vegetation density*

For Beijing city, building density and the ratio of building (1995, 2005, and 2017) were calculated from the training data selected from our land use classification results. Likewise, the spatial average LSTs were counted in the same areas as the training data. Regression analysis, with a high *R*-square correlation coefficient from 1995 to 2017 (see Figure 7a, 7c, and 7e) reveals that there is a positive linear relationship between building density and LST. The *R*-square coefficient increased significantly from 0.4910 in 1995 to 0.7406 in 2017, indicating that building density and LST are more closely related. Furthermore, the slope of their regression curves also increased significantly from 0.1635 to 0.3329, suggesting that building density has a stronger impact on LST and SUHI than rapid urbanization.

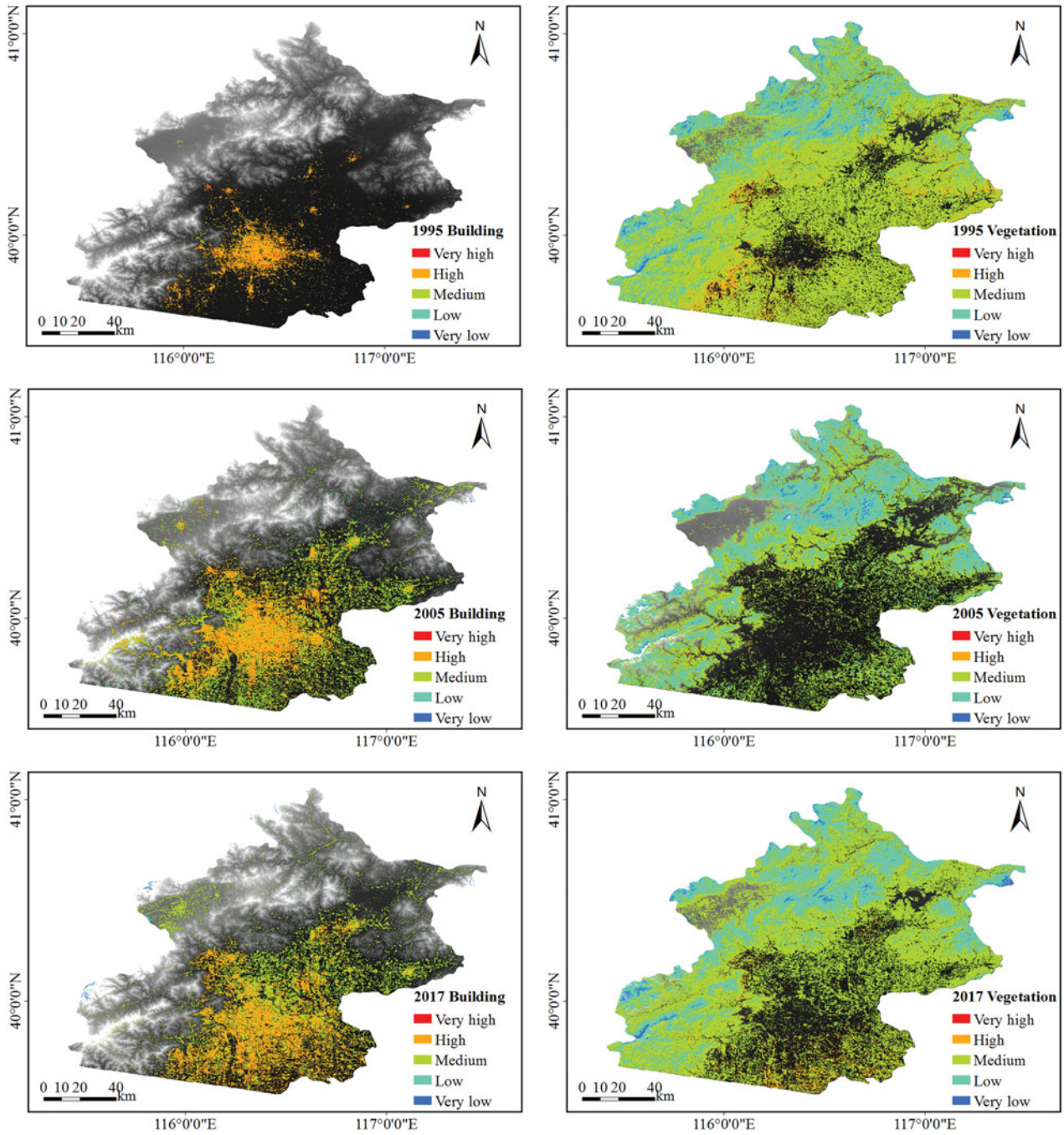


**Figure 4.** Spatial distribution of LST between building and vegetation for 1995, 2005, and 2017.

Notably, on the condition there is a small ratio of buildings in an area, building has little effect on LST. As the city develops, with increasing building density, high-density buildings significantly affect LST, especially in downtown areas.

However, there is a minor phenomenon where the degree of influence of the building density on temperature ceases to increase when the ratio of buildings reaches a certain value, estimated at roughly 25% (see Figure 8). This indicates that there are other factors that affect the changes in surface temperature. The vegetation density of Beijing is characterized by the average NDVI derived from Landsat data by band calculation. A linear regression analysis, conducted between NDVI and LST (see Figure 7b, 7d, and 7f) revealed a negative correlation, indicating vegetation has a relieving effect on SUHI. The regression has a higher *R*-square coefficient of 0.7991 and 0.6459 for 2005 and 2017, respectively.

Likewise, the same as for building density, there is also an important phenomenon: from 1995 to 2017, the regression for NDVI has a steeper slope. The

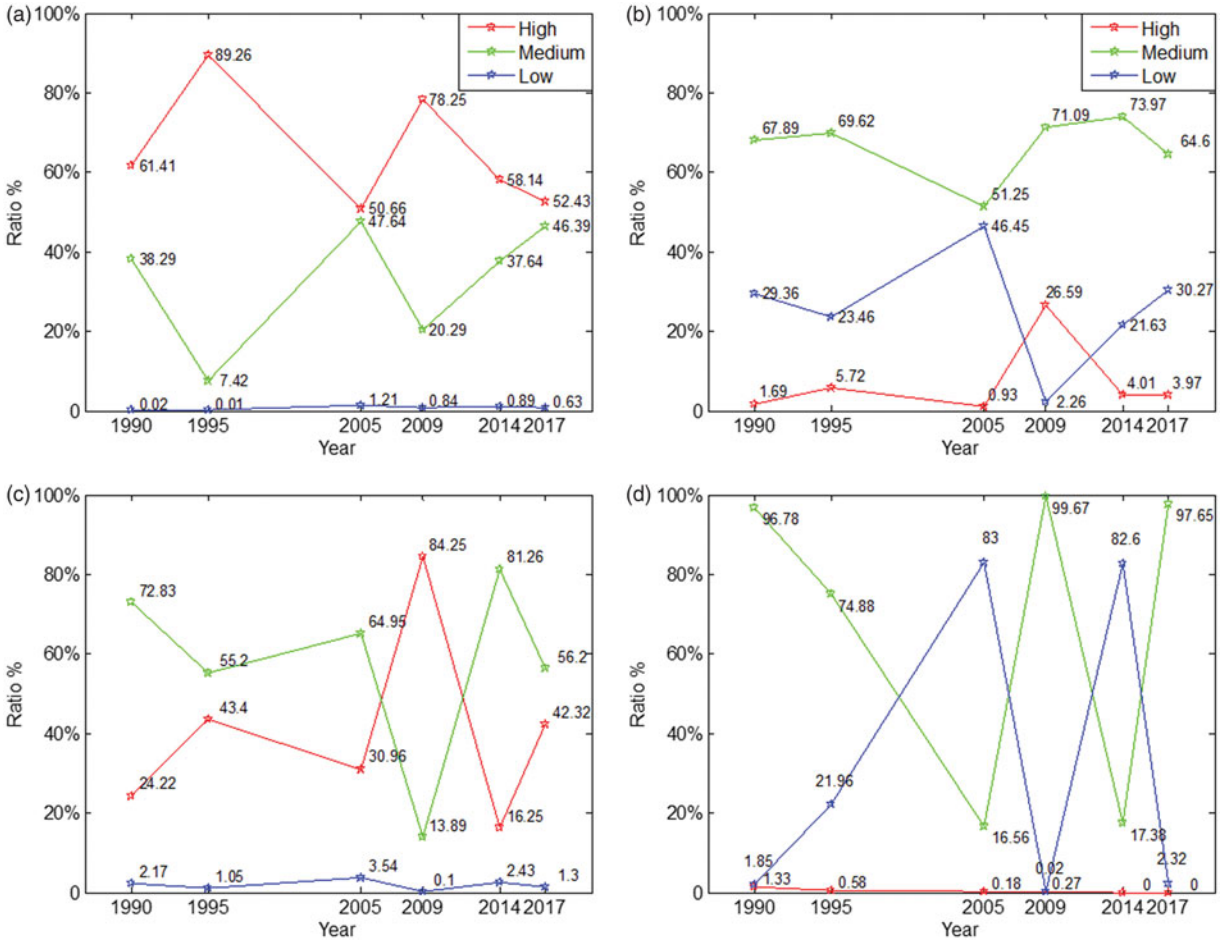


**Figure 5.** Changes in the ratio of high, medium, and low temperature in different land use for building (a), vegetation (b), bare land (c), and water area (d) from 1990 to 2017.

slowly increasing regular pattern shows that vegetation for the city played a more significant role in reducing the urban thermal effect. The high degree of vegetation, reflected by the mean NDVI values within a unit area, has a greater effect in reducing UHI, whereas there is only minimal impact on LST where the area has lower vegetation density or NDVI values ranging from 0 to 0.1.

As seen in Figures 4 and 6, the changes of SUHI intensity and spatial distribution are mainly caused by the change of LULC types, and the SUHI phenomenon with different levels is driven by different factors. The high SUHI is driven by building area, bare land, and workshop building, whereas the low SUHI is driven by vegetation and water area. In the area with high temperature, the proportion of building area has increased while there is little change on the LULC types for the area with medium or low temperature. From 1990 to 2017, the amount of increased building areas leads to high SUHI and the stable amount of vegetation or water areas played a role in reducing and mitigating the SUHI.

In the past few decades, Beijing has experienced rapid urbanization and growth of the urban population, causing an increase in building areas but a decrease in vegetation. With the development of the economy, a large number of factories, buildings, and roads were built, leading to the high SUHI. Meanwhile, the greenhouse effect, resulting from human activities with the emission of greenhouse gases, must be paid attention to. Many measures can be taken to alleviate the growing SUHI effect and the greenhouse effect. A good choice is to consider adjusting the urban ecological structure, such as adding wetlands and green parks, and saving energy and reducing emissions.

### *Temperature profile curves of the regions of interest*

Simply compared with the LSTs in the same area at different times, the changing characteristics and trends are obvious, but it is difficult to explore the interrelationships among adjacent areas. Temperature profiles

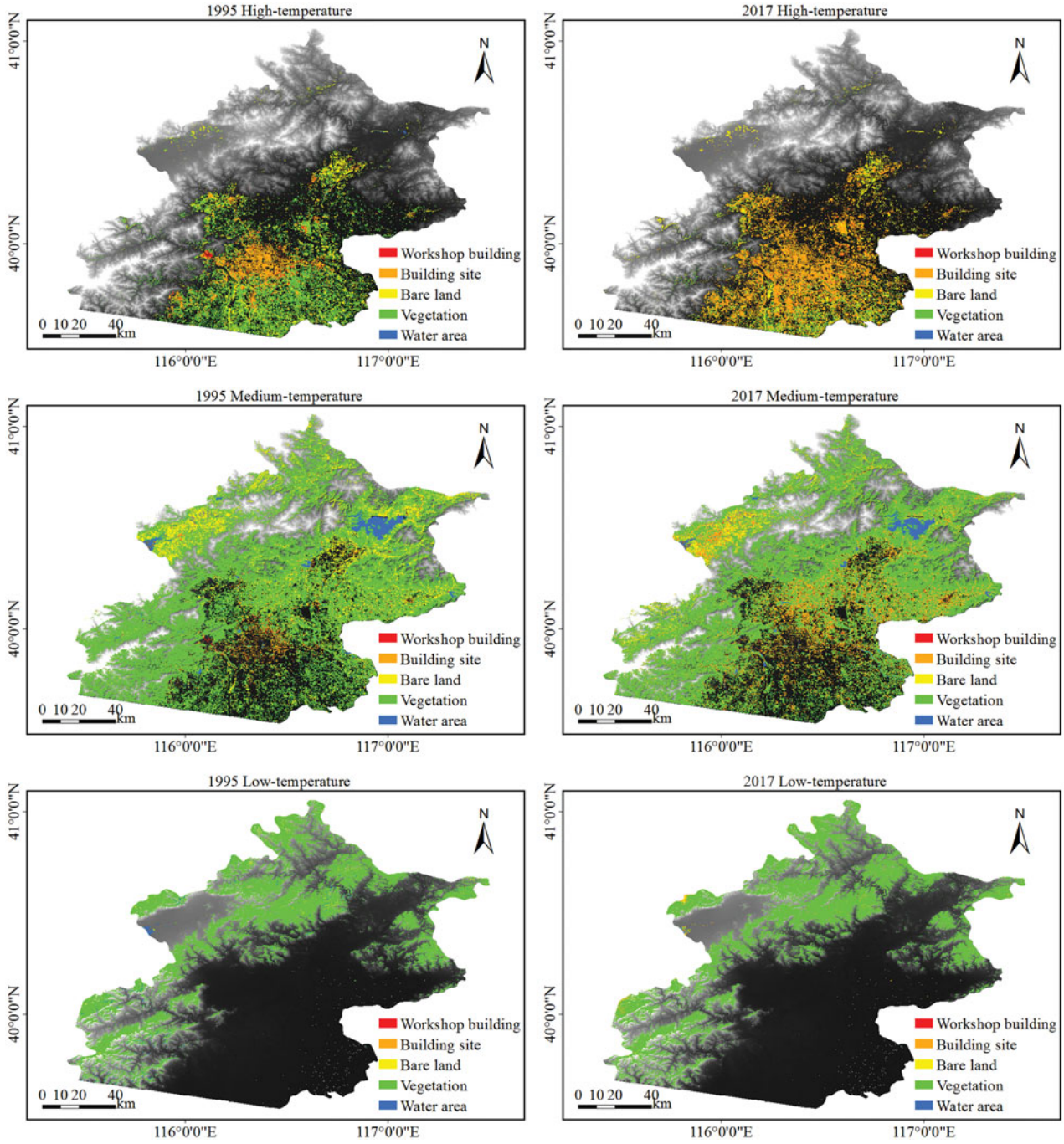


**Figure 6.** Changes in the distribution of LULC type in the area with high, medium, and low temperature in 1995 and 2017.

on the interested path at different times not only include the changing of LSTs, but also reflect the relationship and different change mode between the near areas with the same LST. Spatially, from urban to suburban and rural areas of a megacity, the changes in LSTs indicate the characteristics of development. Figure 9 shows temperature profile curves for one path selected across Beijing from Miyun to Fangshan for 1995 and 2017. In the north-east area of Beijing, LST is significantly lower than in the other regions. The LSTs of some areas, such as Fangshan, increased significantly from 1995 to 2017, creating more serious SUHIs as reflected in Figure 9.

After the water area, from Miyun to Shunyi, the temperature rose sharply, implying a larger transition to the rural area and marking of the boundary of the urban area. Water areas have a lower temperature than the surrounding areas, thereby weakening the

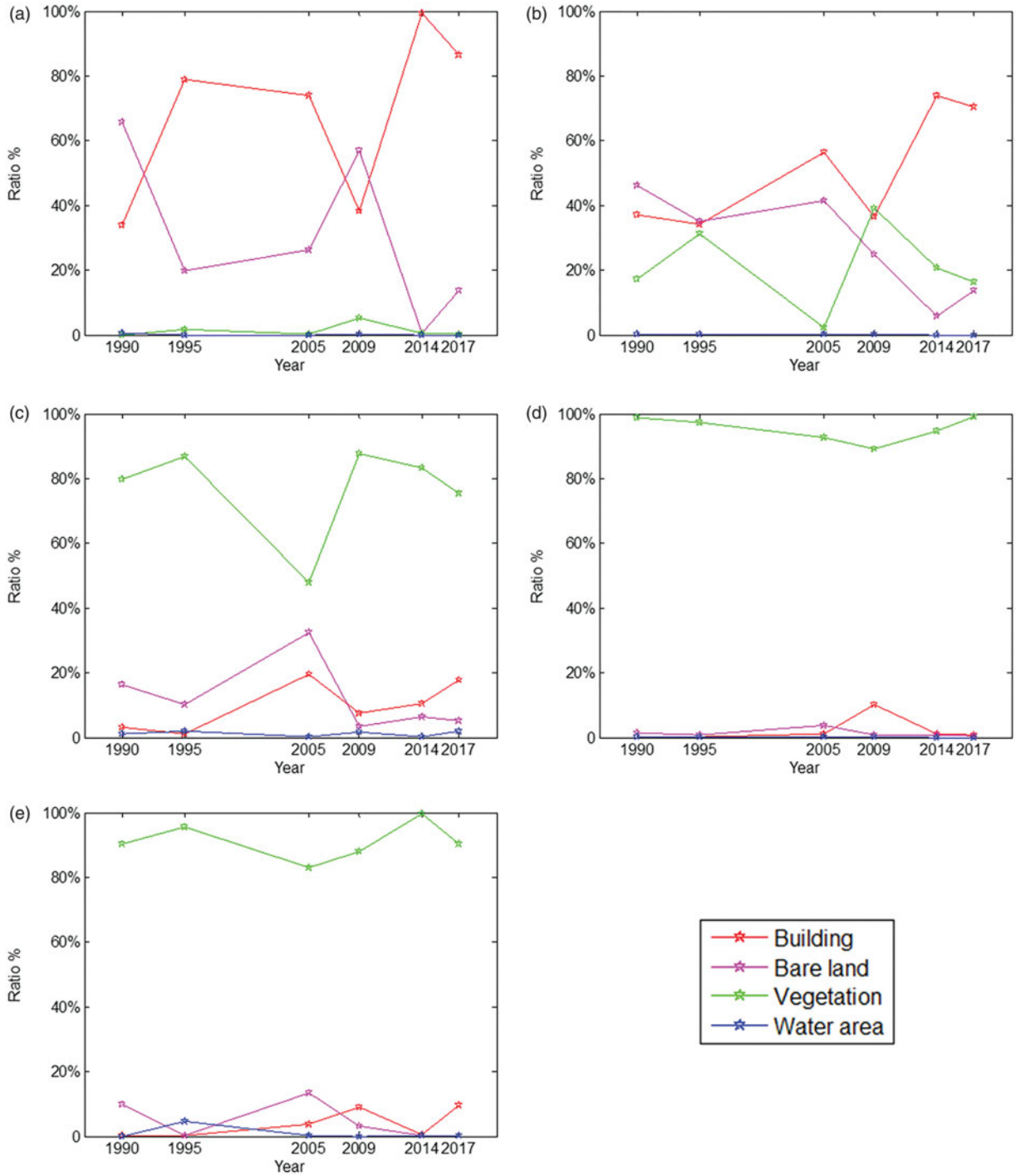


**Figure 7.** Changes in the ratio of building, bare land, vegetation and water areas in different LST levels for very high (a), high (b), medium (c), low (d), and very low (e) from 1990 to 2017.

urban heat island effect in the same way as vegetation does.

### *The evaluation of the quality of the results*

The cloudless Landsat-5 and Landsat-8 images, acquired at about AM 10 o'clock Beijing time, were selected to estimate the LSTs. The acquisition season and time of image reflects the height of the sun, which can also affect LST. However, using the relative LST, here the acquisition time of all images is close (see Table 1) and the difference is negligible. In terms of data quality, the images from 2 satellites are different. TM6 from Landsat-5 and TRIS10 from Landsat-8

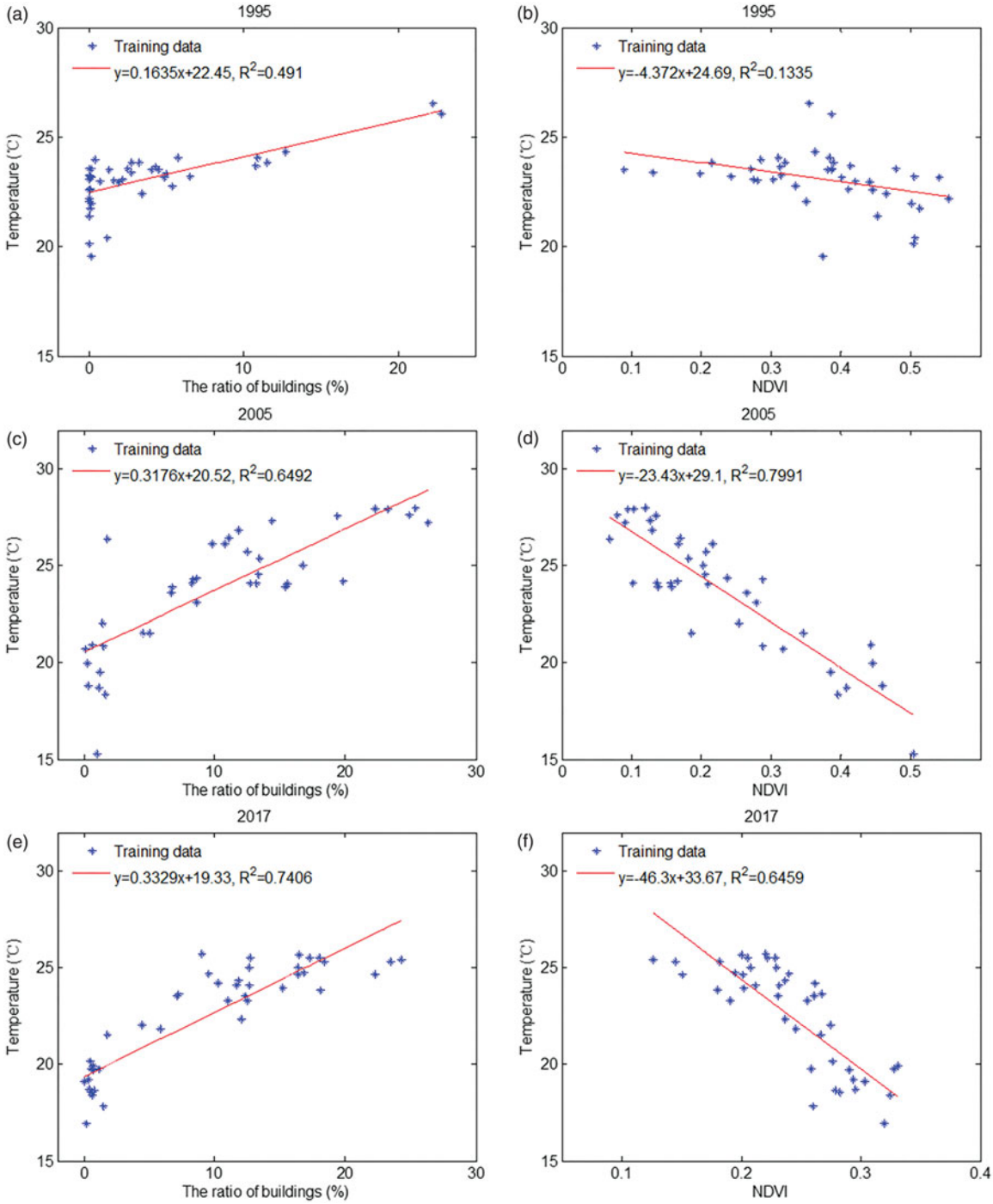


**Figure 8.** Regression analysis curve between building density (a, c and e) or NDVI (b, d and f) and LST for 1995, 2005, and 2017.

are mainly used for the retrieval of LST. However, they are also different in resolution and spectral range; the former has a resolution of 120-m pixel with the spectral range from 10.40 μm to 12.50 μm. The latter has a resolution of 100-m pixel with the spectral range from 10.60 μm to 11.19 μm, whereas the level 1 image data of Landsat acquired from the USGS was selected in the study, with a resolution of 30-m pixel for each band. The same processing method, cubic convolution resampling, does not affect the results of LST.

The 2 LST retrieval methods were selected for different satellite images, with different results for the LST estimations. Meanwhile, the relative LST was adopted to evaluate SUHI intensity and reduce the differences between results from two algorithms. As mentioned in Section 4.1, the differences between results from 2 algorithms, under different LULC, are consistent, which indicates that the similar regression analysis results between LST and NDVI are acquired by 2 methods.

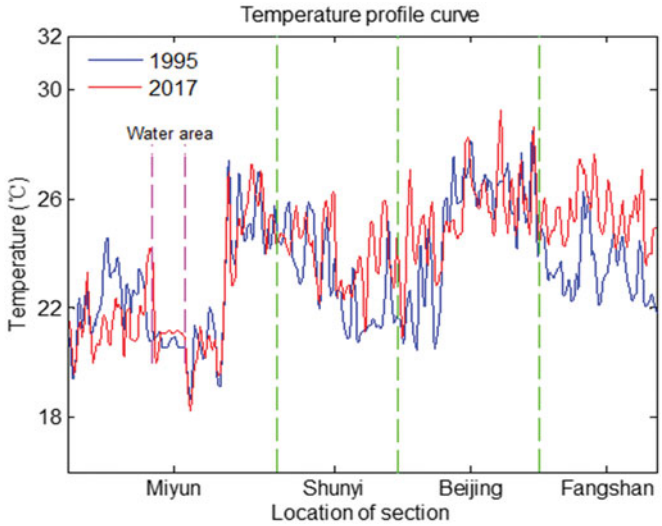


**Figure 9.** Temperature profiles for 1995 and 2017.

The maximum likelihood classification method has been used for the extraction of LULC types. Based on the sample and reference data, the best classification result of each image was selected. Generally, building and vegetation density of images were calculated with high accuracy. In the regression analysis between LST and building or vegetation density, many training sample points were selected to reduce errors due to classification accuracy.

## Conclusion

The LSTs of Beijing were derived from Landsat data. The selected LST data were used to estimate the intensities of SUHI and analyze their spatial distribution and evolution from 1990 to 2017. The LSTs of Beijing are classified into 5 levels, which represent different SUHI intensities. The general trend of changes in LSTs and SUHIs were analyzed and the relationship between LULC and LST were discussed by studying the distribution of LST in the area with the same land use type and characterizing the changing trend of land use type in the area with the same LST.

Building sites, workshop buildings, and bare land were found to be the main reasons for the urban heat island effect, in which building, as inferred by the linear regression analysis between building density and LST, has an increasing trend toward UHI.

For every 1% increase in building density, the increase in the temperature amplitude in 2017 was twice as large as it was in 1995. In terms of NDVI values, the decrease in amplitude of LST in 2017 was 10 times that of the year where there is only a slight increase in the NDVI values of the area. Furthermore, compared to other LULC types, both vegetation and water areas reduce the effect of UHI. Finally, the temperature profile curves for 1995 and 2017 were used to reveal the spatial distribution characteristics of the LSTs and analyze the trend of LST as the result of changing LULC based on the interested regions selected by this study.

## Acknowledgement

This work was supported by the Strategic Priority Research Program of the Chinese Academy of Sciences [XDA23090203], National Key Technologies Research and Development Program of China [2016YFB0502600] and the Key Program of Sichuan Bureau of Science and Technology.

## References

Abbas, S., Nichol, J., Qamer, F., and Xu, J. 2014. "Characterization of drought development through remote sensing: A case study in Central Yunnan, China." *Remote Sensing*, Vol. 6(No. 6): pp. 4998–5018. doi:10.3390/rs6064998.

Alavipanah, S., Wegmann, M., Qureshi, S., Weng, Q., and Koellner, T. 2015. "The Role of vegetation in mitigating urban land surface temperatures: A case study of Munich, Germany during the warm season." *Sustainability*, Vol. 7(No. 4): pp. 4689–4706. doi:10.3390/su7044689.

Bechtel, B. 2015. "A New global climatology of annual land surface temperature." *Remote Sensing*, Vol. 7(No. 3): pp. 2850–2870. doi:10.3390/rs70302850.

Bounoua, L., Zhang, P., Mostovoy, G., Thome, K., Masek, J., Imhoff, M., Shepherd, M., et al. 2015. "Impact of urbanization on US surface climate." *Environmental Research Letters*, Vol. 10(No. 8): pp. 084010. doi:10.1088/1748-9326/10/8/084010.

Chen, L., Jiang, R., and Xiang, W.N. 2016. "Surface heat island in Shanghai and its relationship with urban

development from 1989 to 2013." *Advances in Meteorology*, Vol. 2016(No. 22): pp. 1. doi:10.1155/2016/9782686.

Chen, W., Zhang, Y., Pengwang, C., and Gao, W. 2017. "Evaluation of urbanization dynamics and its impacts on surface heat islands: A case study of Beijing, China." *Remote Sensing*, Vol. 9(No. 5): pp. 453. doi:10.3390/rs9050453.

Choi, Y.Y., Suh, M.S., and Park, K.H. 2014. "Assessment of surface urban heat islands over three megacities in East Asia using land surface temperature data retrieved from COMS." *Remote Sensing*, Vol. 6(No. 6): pp. 5852–5867. doi:10.3390/rs6065852.

Cristóbal, J., Ninyerola, M., and Pons, X. 2008. "Modeling air temperature through a combination of remote sensing and GIS data." *Journal of Geophysical Research Atmospheres*, Vol. 113(No. D13): pp. D13106. doi:10.1029/2007JD009318.

Cui, Y., Xu, X., Dong, J., and Qin, Y. 2016. "Influence of urbanization factors on surface urban heat island intensity:A comparison of countries at different developmental phases." *Sustainability*, Vol. 8(No. 8): pp. 706. doi:10.3390/su8080706.

Estoque, R.C., Murayama, Y., and Myint, S.W. 2017. "Effects of landscape composition and pattern on land surface temperature: An urban heat island study in the megacities of Southeast Asia." *Science of the Total Environment*, Vol. 577: pp. 349–359. doi:10.1016/j.scitotenv.2016.10.195.

Hu, D., Huang, S.L., Feng, Q., Li, F., Zhao, J.J., Zhao, Y.H., and Wang, B.N. 2008. "Relationships between rapid urban development and the appropriation of ecosystems in Jiangyin City, Eastern China." *Landscape & Urban Planning*, Vol. 87(No. 3): pp. 180–191. doi:10.1016/j.landurbplan.2008.06.001.

Huang, C., and Ye, X. 2015. "Spatial modeling of urban vegetation and land surface temperature: A case study of Beijing." *Sustainability*, Vol. 7(No. 7): pp. 9478–9504. doi:10.3390/su7079478.

Jones, P.D., and Lister, D.H. 2010. "The urban heat island in Central London and urban-related warming trends in Central London since 1900." *Weather*, Vol. 64(No. 12): pp. 323–327. doi:10.1002/wea.432.

Kaufmann, R.K., Zhou, L., Myneni, R.B., Tucker, C.J., Slayback, D., Shabanov, N.V., and Pinzon, J. 2003. "The effect of vegetation on surface temperature: A statistical analysis of NDVI and climate data." *Geophysical Research Letters*, Vol. 30(No. 22): pp. 2147. doi:10.1029/2003GL018251.

Knutson, T.R., Delworth, T.L., Dixon, K.W., and Stouffer, R.J. 1999. "Model assessment of regional surface temperature trends (1949–1997)." *Journal of Geophysical Research: Atmospheres*, Vol. 104 (No. D24): pp. 30981–30996. doi:10.1029/1999JD900965.

Kumar, D., and Shekhar, S. 2015. "Statistical analysis of land surface temperature–vegetation indexes relationship through thermal remote sensing." *Ecotoxicology & Environmental Safety*, Vol. 121: pp. 39–44. doi:10.1016/j.ecoenv.2015.07.004.

Liu, L., and Zhang, Y. 2011. "Urban heat island analysis using the Landsat TM data and ASTER data: A case study in Hong Kong." *Remote Sensing*, Vol. 3(No. 7): pp. 1535–1552. doi:10.3390/rs3071535.

Martin, P., Baudouin, Y., and Gachon, P. 2014. "An alternative method to characterize the surface urban heat island." *International Journal of Biometeorology*, Vol. 59(No. 7): pp. 1–13. doi:10.1007/s00484-014-0902-9.

Melaas, E.K., Wang, J.A., Miller, D.L., and Friedl, M.A. 2016. "Interactions between urban vegetation and surface urban heat islands: a case study in the Boston metropolitan region." *Environmental Research Letters*, Vol. 11(No. 5): pp. 054020. doi:10.1088/1748-9326/11/5/054020.

Ogashawara, I., and Bastos, V.D.S.B. 2012. "A quantitative approach for analyzing the relationship between urban heat islands and land cover." *Remote Sensing*, Vol. 4(No. 11): pp. 3596–3618. doi:10.3390/rs4113596.

Orhan, O., Ekercin, S., and Dadaser-Celik, F. 2014. "Use of Landsat land surface temperature and vegetation indices for monitoring drought in the Salt Lake Basin Area, Turkey." *The Scientific World Journal*, Vol. 2014: pp. 1. doi:10.1155/2014/142939.

Purwanto, P., Utomo, D.H., and Kurniawan, B.R. 2016. "Spatio temporal analysis trend of land use and land cover change against temperature based on remote sensing data in Malang City." *Procedia - Social and Behavioral Sciences*, Vol. 227: pp. 232–238.

Qin, Z.H., Li, W.J., Zhang, M.H., Karnieli, A., and Berliner, P. 2003. "Estimating of the essential atmospheric parameters of mono-window algorithm for land surface temperature from Landsat TM6." *Remote Sensing for Land & Resources*, Vol. 15(No. 2): pp. 37–43. doi:10.6046/gtzyyg.2003.02.10.

Qin, Z.H., Li, W.J., Bin, X.U., Chen, Z.X., and Liu, J. 2004. "The estimation of land surface emissivity for Landsat TM6." *Remote Sensing for Land & Resources*, Vol. 16(No. 3): pp. 28–32.

Qin, Z.H., Zhang, M.H., Karnieli, A., and Berliner, P. 2001. "Mono-window algorithm for retrieving land surface temperature from landsat tm6 data." *Acta Geographica Sinica*, Vol. 56(No. 4): pp. 456–466.

Ranagalage, M., Estoque, R.C., and Murayama, Y. 2017. "An urban heat island study of the Colombo Metropolitan Area, Sri Lanka, based on Landsat data (1997–2017)." *ISPRS International Journal of Geo-Information*, Vol. 6(No. 7): pp. 189. doi:10.3390/ijgi6070189.

Rinner, C., and Hussain, M. 2011. "Toronto's urban heat island - exploring the relationship between land use and surface temperature." *Remote Sensing*, Vol. 3(No. 6): pp. 1251–1265. doi:10.3390/rs3061251.

Şahin, M. 2012. "Modelling of air temperature using remote sensing and artificial neural network in Turkey." *Advances in Space Research*, Vol. 50(No. 7): pp. 973–985. doi:10.1016/j.asr.2012.06.021.

Song, J., Wang, Z.H., Myint, S.W., and Wang, C. 2017. "The hysteresis effect on surface-air temperature relationship and its implications to urban planning: An examination in Phoenix, Arizona, USA." *Landscape & Urban Planning*, Vol. 167: pp. 198–211. doi:10.1016/j.landurbplan.2017.06.024.

Tomlinson, C.J., Chapman, L., Thornes, J.E., and Baker, C. 2011. "Remote sensing land surface temperature for meteorology and climatology: A review." *Meteorological*

*Applications*, Vol. 18(No. 3): pp. 296–306. doi:10.1002/met.287.

Urban, M., Eberle, J., Hüttich, C., Schmullius, C., and Herold, M. 2013. "Comparison of satellite-derived land surface temperature and air temperature from meteorological stations on the pan-Arctic scale." *Remote Sensing*, Vol. 5(No. 5): pp. 2348–2367. doi:10.3390/rs5052348.

Van, T.T., and Bao, H.D.X. 2010. "Study of the impact of urban development on surface temperature using remote sensing in Ho Chi Minh City, Northern Vietnam." *Geographical Research*, Vol. 48(No. 1): pp. 86–96.

Wang, H., Zhang, Y., Tsou, J., and Li, Y. 2017. "Surface urban heat island analysis of Shanghai (China) based on the change of land use and land cover." *Sustainability*, Vol. 9(No. 9): pp. 1538. doi:10.3390/su9091538.

Wei, Y.D., and Ye, X. 2014. "Urbanization, land use, and sustainable development in China." *Stochastic Environmental Research and Risk Assessment*, Vol. 28(No. 4): pp. 755–755. doi:10.1007/s00477-013-0820-0.

Xu, H., Lin, D., and Tang, F. 2013. "The impact of impervious surface development on land surface temperature in a subtropical city: Xiamen, China." *International Journal of Climatology*, Vol. 33(No. 8): pp. 1873–1883. doi:10.1002/joc.3554.

Ye, C.M., Wang, M.J., and Li, J. 2017. "Derivation of the characteristics of the surface urban heat island in the Greater Toronto Area using thermal infrared remote sensing." *Remote Sensing Letters*, Vol. 8(No. 7): pp. 637–646. doi:10.1080/2150704X.2017.1312025.

Yu, X., Guo, X., and Wu, Z. 2014. "Land surface temperature retrieval from Landsat 8 TIRS—comparison between radiative transfer equation-based method, split window algorithm and single channel method." *Remote Sensing*, Vol. 6(No. 10): pp. 9829–9852. doi:10.3390/rs6109829.

Zareie, S., Khosravi, H., Nasiri, A., and Dastorani, M. 2016. "Using Landsat Thematic Mapper (TM) sensor to detect change in land surface temperature in relation to land use change in Yazd." *Iran." Solid Earth*, Vol. 7(No. 6): pp. 1551–1564. doi:10.5194/se-7-1551-2016.

Zhou, C., Wang, K., and Ma, Q. 2017. "Evaluation of eight current reanalyses in simulating land surface temperature from 1979 to 2003 in China." *Journal of Climate*, Vol. 30(No. 18): pp. 7379–7398. doi:10.1175/JCLI-D-16-0903.1.

Zipper, S.C., Schatz, J., Singh, A., Kucharik, C.J., Townsend, P.A., and Loheide, S.P. 2016. "Urban heat island impacts on plant phenology: Intra-urban variability and response to land cover." *Environmental Research Letters*, Vol. 11(No. 5): pp. 054023. doi:10.1088/1748-9326/11/5/054023.